

**UCLA**

**UCLA Electronic Theses and Dissertations**

**Title**

Quantifying the phenotypic information in mRNA and receptor complex abundances

**Permalink**

<https://escholarship.org/uc/item/6ft5h0n5>

**Author**

Maltz, Evan

**Publication Date**

2022

**Supplemental Material**

<https://escholarship.org/uc/item/6ft5h0n5#supplemental>

Peer reviewed|Thesis/dissertation

UNIVERSITY OF CALIFORNIA

Los Angeles

Quantifying the phenotypic information in mRNA and receptor complex abundances

A dissertation submitted in partial satisfaction of the requirements for the degree Doctor of  
Philosophy in Biochemistry, Molecular and Structural Biology

by

Evan Maltz

2022

© Copyright by

Evan Maltz

2022

## ABSTRACT OF THE DISSERTATION

Quantifying the phenotypic information in mRNA and receptor complex abundances

by

Evan Maltz

Doctor of Philosophy in Biochemistry, Molecular and Structural Biology

University of California, Los Angeles, 2022

Professor Roy Wollman, Chair

Quantifying the dependency between biomolecular composition and downstream cellular phenotypes is a fundamental open problem in biology. Advances in multimodal single cell measurement technologies provide an opportunity to apply new computational frameworks to dissect the contribution of individual and combinations of biomolecules to a given phenotype. In this work, I analyzed complex relationships related to transcriptional activity, receptor abundance, apoptotic decisions, and  $\text{Ca}^{2+}$  signaling. In the first chapter, I used an information theory approach to analyze multimodal data of the expression of 83 genes in the  $\text{Ca}^{2+}$  signaling network and the dynamic  $\text{Ca}^{2+}$  response in the same cell. We found that the overall expression levels of these 83 genes explain approximately 60% of  $\text{Ca}^{2+}$  signal entropy. The average contribution of each single gene was 17%, revealing a large degree of redundancy between genes. In the second chapter, I connect apoptotic decision-making to transcriptional activity, receptor abundance, and caspase activity. In both approaches, I quantify relationships between cell state and phenotype from multimodal, high-dimensional data.

The dissertation of Evan Maltz is approved.

Alexander Hoffmann

Albert Courey

Margot Quinlan

Roy Wollman, Committee Chair

## DEDICATION

To my family and teachers, for giving me the opportunity to pursue my dreams.

TABLE OF CONTENTS

ABSTRACT OF THE DISSERTATION .....ii

DEDICATION .....iv

TABLE OF CONTENTS .....v

LIST OF FIGURES .....vi

ACKNOWLEDGMENTS .....vii

VITA ..... ix

CHAPTER 1 - Quantifying the phenotypic information in mRNA abundance ..... 1

    Abstract ..... 1

    Introduction..... 1

    Results ..... 8

    Discussion ..... 17

    Methods ..... 20

    Acknowledgments ..... 22

    References ..... 23

CHAPTER 2 - Predicting Death Decisions from Signaling Dynamics ..... 29

    Abstract. .... 35

    Introduction..... 29

    Results. .... 31

    Discussion ..... 33

    Materials and Methods ..... 34

    Acknowledgments..... 35

    References ..... 35

CONCLUSIONS..... 36

## LIST OF FIGURES

<b>Figure 1.1</b> Structure of Gene and Ca <sup>2+</sup> Data .....	10
<b>Figure 1.2</b> Mutual Information Between Individual Genes and Ca <sup>2+</sup> Signals.....	12
<b>Figure 1.3</b> Synergy and Redundancy of Gene Pairs with Respect to Ca <sup>2+</sup> .....	14
<b>Figure 1.4</b> Mutual Information Between Gene Sets and Ca <sup>2+</sup> Signals.....	17
<b>Figure 2.1</b> DISC Connects Transcription and Death Decision Timing.....	31
<b>Figure 2.2</b> Predicting Death from Caspase 8 Activity Over Time .....	33



## ACKNOWLEDGMENTS

This paper is the result of the hard work, generosity, and support of so many people. I'm incredibly grateful for the support I've received from the Cellular and Molecular Biology Training Grant and Whitcome Fellowship, which gave me the independence to focus on my research. Additionally, the NVIDIA Corporation generously provided 2 Titan V GPUs, without which most of my research would not be possible. NVIDIA's GPU grants program allowed me to pursue machine learning both as a student and a career.

I'd like to thank QCBio for all of the constructive feedback, meetings, conferences, and opportunities they've provided me. Importantly, Alex Hoffmann and Eric Deeds have been such valuable mentors with significant contributions to my work and understanding of information theory, cellular biology, signaling, and machine learning. I especially want to thank Eric Deeds for hosting a book club where we really took a deep dive into machine learning theory, and also for always having thoughtful, constructive questions after every presentation; without your suggestion to apply my approach on a toy model, I don't think I would have ever solved it. And thank you to Margot Quinlan and Albert Courey for their support on my committee.

I'm also sincerely grateful to all of the research mentors who have helped and taught me. Adewunmi Adelaja was always so helpful and knowledgeable during my rotation in the Hoffmann lab and as a collaborator. And thank you to Rob Foreman who helped me so much in formulating my project, providing me the data, teaching me the protocols, guiding my programming skills, and pushing me to persevere. I want to thank Jennifer Oyler-Yaniv for being a fantastic mentor throughout my experience, especially teaching me the process of scientific writing and always providing feedback on my proposals; the journal club she organized taught me more about research than anything else, and her support in the lab designing experiments was so incredibly valuable to my thought process as a scientist. And I'd also like to sincerely thank Alon Oyler-Yaniv for teaching me about statistics, programming,

and data analysis; I'm so grateful for all the feedback on my writing, presentations, and experiments/analysis which have been so useful to me and my career.

I would like to give a special thank you to my advisor and mentor, Roy Wollman. He gave me the opportunity to explore my interests and develop my skills to their fullest potential. I am incredibly grateful to him for everything he has taught me, including data science, machine learning, information theory, statistics, and the essential skills of research. Roy has been an incredible support throughout my graduate career, and I have had an immensely rewarding and fulfilling experience in his lab. I'd like to specifically thank Zach Hemminger and Maeve Nagle for all their help. And finally, I'd like to thank the entire Wollman Lab for their support, feedback, and friendship over the years because I could not have done it without you all.

## VITA

- 2014 - 2017      B.S. in Biochemistry and Molecular Biology, University of Wisconsin-Madison, WI
- 2017 - 2019      M.S. in Biochemistry, Molecular and Structural Biology, University of California at Los Angeles, Los Angeles, CA

## PUBLICATIONS

Nagle, M. P., Tam, G. S., **Maltz, E.**, Hemminger, Z., & Wollman, R. Bridging scales: From cell biology to physiology using *in situ* single-cell technologies. *Ce// Syst* **12**, 388-400 (2021)

Oyler-Yaniv, J., Oyler-Yaniv, A., **Maltz, E.**, & Wollman, R. TNF controls a speed-accuracy tradeoff in the cell death decision to restrict viral spread. *Nature communications* 12.1, 1-11 (2021)

**Maltz, E.**, & Wollman, R. Quantifying the phenotypic information in mRNA abundance. *bioRxiv*. Preprint. (2022)

## CHAPTER 1

### *Quantifying the phenotypic information in mRNA abundance*

#### **Abstract**

Quantifying the dependency between mRNA abundance and downstream cellular phenotypes is a fundamental open problem in biology. Advances in multimodal single cell measurement technologies provide an opportunity to apply new computational frameworks to dissect the contribution of individual genes and gene combinations to a given phenotype. Using an information theory approach, we analyzed multimodal data of the expression of 83 genes in the  $\text{Ca}^{2+}$  signaling network and the dynamic  $\text{Ca}^{2+}$  response in the same cell. We found that the overall expression levels of these 83 genes explain approximately 60% of  $\text{Ca}^{2+}$  signal entropy. The average contribution of each single gene was 17%, revealing a large degree of redundancy between genes. Using different heuristics, we estimated the dependency between the size of a gene set and its information content, revealing that on average a set of 53 genes contains 54% of the information about  $\text{Ca}^{2+}$  signaling. Our results provide the first direct quantification of information content about complex cellular phenotype that exists in mRNA abundance measurements.

#### **Introduction**

Cellular phenotypes emerge from many regulated interactions between various components. Rates of synthesis and degradation determine the instantaneous abundances of different biological molecules. These kinetic rates are themselves a property of regulatory interactions between biomolecules creating multilayered feedback networks (El-Samad, 2021). Both the dynamic and instantaneous abundances of biomolecules are key determinants of cellular phenotypes, underlying their ability to make different decisions given the same stimulus (Purvis & Lahav, 2013; Perkins & Swain, 2009; Cheong *et al*, 2011). The ability to systematically measure the abundance of large sets of different biomolecules such as mRNA and proteins enables the

determination of regulatory strengths across different nodes of these complex networks. Pioneering work in *E. coli* based on instantaneous single cell measurements of mRNA and protein copy numbers reveal a surprisingly low correlation coefficient of  $r=0.01 \pm 0.03$  across 129 highly expressed genes (Taniguchi *et al*, 2010). The lack of correlation between mRNA and protein in *E. coli* might be due to their small size and magnitude of temporal fluctuation in mRNA levels. However, more recent advances in multimodal assays in mammalian cells also identified low correlations between the abundances of most proteins and corresponding mRNAs (Stoeckius *et al*, 2017; Gong *et al*, 2017; Schulz *et al*, 2018; Mair *et al*, 2020; Darmanis *et al*, 2016). This low correlation appears to contradict intuition that protein and mRNA levels should strongly correspond within cells because of the dependency suggested by the central dogma (Liu *et al*, 2016). An alternative hypothesis is that the majority of regulatory steps and phenotypically relevant information lie in post transcriptional processes. Post-transcriptional regulation can modulate both protein activity and abundance via protein interactions, post-translational modifications, RNA interactions/structure, and more. Stochastic processes also obscure the importance of molecular composition to phenotypic outcomes (Balázsi *et al*, 2011; Perkins & Swain, 2009; Cheong *et al*, 2011). Yet, many studies have pointed to differences in mRNA levels among clonal cells to explain differences in cellular phenotypes (Shaffer *et al*, 2020; Emert *et al*, 2021). These observations highlight a need for a better framework to address fundamental questions: Does mRNA abundance matter? What fraction of the information about cellular phenotype is determined by mRNA abundance, and what fraction is due to post-transcriptional regulation?

Quantifying the information content in mRNA abundance about cellular phenotypes is technically and computationally challenging due to the many layers of complex interactions in cellular networks (Macaulay *et al*, 2017). Phenotypic information displayed in clonal cells is controlled by molecular composition, stochastic factors, intermediate regulation, and crosstalk (Azeloglu & Iyengar, 2015). Many approaches have been developed to disentangle these complex and distributed dependencies. Feature engineering has been one powerful tool to reveal

interpretable characteristics of signaling dynamics, finding multiple motifs that encode information about stimulus dose and type (Adelaja *et al*, 2021; Zhang *et al*, 2017; Wong *et al*, 2019; Hafner *et al*, 2017; Nelson *et al*, 2004). However, these features do not capture all the information in complex dynamics, which are difficult to study and fully recapitulate in mechanistic models (Myers *et al*, 2021). Another common approach is to perform dimensionality reduction and/or clustering to integrate different modalities (Subramanian *et al*, 2020; Kinnunen *et al*, 2021). Several studies have clustered groups of genes or cells based on signal patterns to reveal general mechanisms of how signaling dynamics affect transcription (Lane *et al*, 2017; Hafner *et al*, 2017). However, it is still unknown how differences in arbitrary sets of transcripts relate to dynamic signals in the same cells. Signaling phenomena may emerge due to differences among many combinations of genes, which may be missed when simplified to either individual genes or gene clusters. Single-cell network states are notoriously difficult to fully measure, and insights about the relationships between many components requires high dimensional and multimodal data from the same cells (Adelaja *et al*, 2021; Spencer *et al*, 2009; Azeloglu & Iyengar, 2015; Macaulay *et al*, 2017). Although useful in many contexts, feature engineering, clustering, and dimensionality reduction are not guaranteed to capture all useful information.

Directly quantifying the relationship between many transcripts and a phenotype via an information theoretic approach can provide a direct measure of the importance of mRNA abundance. However, three challenges prevent the general use of information theory in quantifying information content in RNA abundance. 1) Biological feedbacks entangle mRNA abundance and cellular phenotype. Cellular phenotypes that emerge over long timescale, e.g., cellular differentiations, have a longer timescale than the lifetime of mRNA molecules that potentially determine the emerging phenotypes. In these cases, mRNA abundances themselves change dynamically adding additional complexities. 2) Quantification of importance of mRNA abundance requires paired measurements of mRNA and the emerging cellular phenotype in question, measurements that are technically challenging due to the destructive nature of mRNA

quantification methods. 3) The statistical measures needed to answer these questions, entropy and mutual information, are notoriously hard to infer. Below, we discuss how these challenges could be addressed to provide direct quantification of the information content in mRNA abundance.

$\text{Ca}^{2+}$  signaling is a useful model system to quantify the dependency between mRNA abundance and emerging cellular phenotypes.  $\text{Ca}^{2+}$  signaling is a system in which the emerging phenotype is faster than changes in mRNA abundance. This timescale separation allows us to assume mRNA abundances are at a quasi-steady state and do not change significantly during the experiment. The dynamics of the  $\text{Ca}^{2+}$  signaling response to ATP is a well-studied model system for environmental sensing, featuring one of the most ubiquitous and multifunctional pathways across cell types. An important role of  $\text{Ca}^{2+}$  signaling is the coordination of responses to changes in extracellular environment. In the physiological context of tissues, cell lysis causes an unusual local increase in extracellular ATP, among other molecules. This type of damage sensing relies on the purinergic cell surface receptors, P1 and P2, which detect adenosine and ATP respectively (Alves *et al*, 2018). The P2Y GPCR triggers a downstream signaling cascade via protein interactions.  $\text{G}_q$ -GTP is released from the P2Y receptor where it can then bind to and activate phospholipase C ( $\text{PLC}\beta$ ).  $\text{PLC}\beta$  cleaves  $\text{PIP}_2$  into  $\text{IP}_3$  and DAG, which facilitate signaling by binding to their respective receptors,  $\text{IP}_3\text{R}$  and DAGR. The  $\text{IP}_3\text{R}$  is embedded in the membrane of the endoplasmic reticulum and functions as a gated  $\text{Ca}^{2+}$  channel that releases  $\text{Ca}^{2+}$  into the cytoplasm upon  $\text{IP}_3$  binding. Cytoplasmic  $\text{Ca}^{2+}$  concentrations are kept relatively low at 50-100nM and spike up to 1uM during signaling with significant and rapid fluctuations producing unique dynamics in every cell (Bagur & Hajnóczky, 2017). Changes in cytoplasmic  $\text{Ca}^{2+}$  concentration over time (i.e., its signaling dynamics) have many emergent features like oscillations caused by coupling between positive and negative feedback loops (Azeloglu & Iyengar, 2015). Studies have shown these dynamics specifically propagate relevant environmental and stimulus information (Selimkhanov *et al*, 2014). While in the cytoplasm,  $\text{Ca}^{2+}$  regulates many signaling molecules, e.g., kinases and phosphatases, through direct binding to  $\text{Ca}^{2+}$  binding domains such as the EF-hand and through

binding to calmodulin isoforms that enables it to activate kinases like protein kinase C. These kinases affect many downstream transcriptional and protein-mediated responses that ultimately regulate cell behavior. The timescale of  $\text{Ca}^{2+}$  dynamics is significantly faster than the timescale of gene expression differentiation, allowing us to interpret a symmetric measure of dependency, such as mutual information, in a directed manner (Putney, 2012). Overall, the  $\text{Ca}^{2+}$  signaling pathway is a complex network with regulation at transcriptional and post-transcriptional levels, providing us with a great model system to dissect the phenotypic information content in mRNA abundances.

Precise measurements of dynamic single-cell, multimodal data have been collected to address these questions. Studies featuring multiomic image-based measurements have mostly focused on fixed cell measurements like immunofluorescence, spatial arrangement of cells in tissues, and chromatin structure (Wang *et al*, 2018; Zhang *et al*, 2021; Liu *et al*, 2021). Studies that have involved dynamic phenotypes were limited by the low sensitivity of scRNAseq (Lane *et al*. 2017) or had to focus on only a handful of genes (Lee *et al*. 2014). Nonetheless, methods are being developed to integrate live cell dynamics and reliable RNA quantification of hundreds of genes (Foreman & Wollman, 2020; Genshaft *et al*, 2021). Measuring the transcriptional state of the  $\text{Ca}^{2+}$  signaling pathway requires the quantification of the abundance of hundreds of genes. Multiplexed Error-Robust Fluorescence In Situ Hybridization (MERFISH) has been developed as a high-throughput, single-cell method for accurately counting large numbers of transcripts (Moffitt *et al*, 2016). Because it is performed in situ, MERFISH can be combined with other imaging methods to create high dimensional, multimodal data consisting of both dynamic and instantaneous measurements. Combining transcriptomic and live-cell data offers unique insights into the role of dynamic regulation and sources of phenotypic information. The challenge of collecting high-dimensional, single cell, paired transcriptomic and signaling dynamics data has been successfully addressed in recent work (Foreman & Wollman, 2020). There, we demonstrated a single cell method for collecting paired measurements of live  $\text{Ca}^{2+}$  signaling dynamics and relevant gene expression using MERFISH. In that work, non-transformed epithelial cells that express a  $\text{Ca}^{2+}$



biosensor were activated with extracellular ATP, imaged for 13 minutes, and fixed for mRNA abundance quantification using MERFISH. Pairing of cells between the two modalities of the experiment created a unique dataset of 5128 cells with 314 timepoints of  $\text{Ca}^{2+}$  signaling dynamics and counts for 83 transcripts. This dataset was the basis for the work described here.

New analytical frameworks have emerged for understanding complex dependencies in multimodal measurements with intractable data distributions. Information theory provides a powerful analytical framework for understanding the relationship between system structure and output (Brennan *et al*, 2012). Shannon's mutual information is a statistical approach for measuring the magnitude of shared, or symmetric, information between two random variables. This framework is powerful because it captures nonlinear relationships and measures true dependence in absolute terms, though it has been difficult to apply to biochemical systems without strict assumptions about the data distribution (Tostevin & ten Wolde, 2010; Uda *et al*, 2013). However, multiomic measurements of single cells often involve different data types that are difficult to relate, that is to define a joint probability distribution. In the case of  $\text{Ca}^{2+}$  signaling networks, signaling data is sampled from a continuous process whereas RNA abundances are discrete. Many paradigms rely on separate analysis of each data type, often via dimensionality reduction or clustering, before relationships can be quantified (Fang *et al*, 2021; Lee *et al*, 2020; Welch *et al*, 2019). While other approaches (e.g., binning or kernel-density estimation) exist for defining a joint probability distribution over some data types, they fail to perform well outside of strict assumptions about the distributions (e.g., gaussianity) or limited dimensionality; a general, scalable approach is necessary to reduce the need for complex and highly specific analytical pipelines that have emerged (Gayoso *et al*, 2021; Zuo & Chen, 2021). Highly flexible neural networks have demonstrated their ability to estimate characteristics of these probability distributions to allow a deeper understanding of the statistical and information theoretic properties of the data. Deep learning has proven useful for classification of and feature generation from ERK and Akt signaling dynamics (Jacques *et al*, 2021). However, direct interpretation of latent embeddings in these neural network outputs is

challenging. An alternative use of deep learning methodologies is a universal functional approximator where neural networks are used to approximate unknown functions to achieve different objective functions. This approach was codified within variational inference and has been proven very useful in probability estimates (Blei et al. 2016). For complex data of mixed types where mutual information is analytically intractable, optimization of neural network functional approximator could be used to find a lower bound. This approach was recently demonstrated under the name Mutual Information Neural Estimator (MINE), which uses a deep neural network to learn a function that can encode the data and find a tight lower bound on the mutual information (Belghazi *et al*, 2018). Briefly, MINE is a universal function approximator that searches for a mapping function  $T$  in a large space of encoder functions parameterized by  $\theta$ .  $T$  maps the data consisting of mRNA counts and  $Ca^{2+}$  signal dynamics,  $G$  and  $Ca^{2+}$  respectively, of arbitrary dimensionality such that  $T_\theta : (G, Ca^{2+}) \rightarrow \mathbb{R}$ . Remarkably, the data require no significant transformations, MINE is simply trained on the raw data because all transformations required for an efficient mapping are theoretically learnable by a model with enough parameters and samples. Letting  $\mathbb{P} := \mathbb{P}_{G, Ca^{2+}}$  represent the joint probability, i.e., paired data, and  $\mathbb{Q} := \mathbb{P}_G \otimes \mathbb{P}_{Ca^{2+}}$  represent the product of the marginal probabilities, i.e., independently sampled data, the mutual information between  $G$  and  $Ca^{2+}$  is the distance between the joint and marginal distributions. This distance is measured using the Kullback-Leibler divergence ( $D_{KL}$ ), and a stronger relationship between  $G$  and  $Ca^{2+}$  is equivalent to a greater distance between the joint and marginals:  $I(G, Ca^{2+}) = D_{KL}(\mathbb{P}||\mathbb{Q})$ . Using the Donsker-Varadhan representation of the  $D_{KL}$ , the model parameters  $\theta$  are optimal when gradient ascent has maximized  $\mathbb{E}_{\mathbb{P}}[T_\theta] - \log(\mathbb{E}_{\mathbb{Q}}[e^{T_\theta}]) \leq D_{KL}(\mathbb{P}||\mathbb{Q})$ , where  $\mathbb{E}$  denotes the expected value. This estimate represents a lower bound on the mutual information. MINE is highly flexible because it makes almost no assumptions about the structure of the data. MINE searches through a large function space for the optimal transformation function to encode the data types assuming there are enough

samples to constrain the model. The result is a lower-bound estimate of the mutual information between paired modalities of almost any dimensionality and complexity.

The recent technological development in multiplexed single cell measurements and machine learning approaches for the inference of mutual information could be integrated to provide direct quantification of the phenotypic information content of mRNA abundances. Here, we utilize these developments and focus on a model with timescale separation between an emerging phenotype and mRNA abundance. We relied on highly multiplexed FISH-based quantification of mRNA levels that is more accurate than sequencing-based approaches and also allows integration with other imaging modalities. Inference of mutual information was done using the  $\text{Ca}^{2+}$  signaling network as a model; we fit MINE on various subsets of 83 genes and 314  $\text{Ca}^{2+}$  timepoints to quantify the contribution of transcript abundance to signaling dynamics. To establish a baseline, we first calculated the dependency between individual genes and  $\text{Ca}^{2+}$  signals. We then calculated the mutual information between gene pairs and  $\text{Ca}^{2+}$  signals to account for redundancy. Gene sets of all sizes were then sampled using various strategies to measure how information changes with set size. Using PCA, we evaluate how useful phenotypic information accounts for transcript-level variance. Overall, we demonstrate a new information theoretic framework for analyzing paired single cell data that provide a quantification of the dependency between sets of mRNAs and an emergent cell-scale dynamic phenotype.

## Results

To investigate the information content of transcript counts and dynamic  $\text{Ca}^{2+}$  signals, we first analyzed each modality on their own.  $\text{Ca}^{2+}$  signals display significant heterogeneity across cells (Fig 1.1A). Likewise, most transcripts had a large range of abundances across cells, though distributions varied depending on the transcript. Pairwise correlation coefficients were calculated for 83 genes across 5128 cells (Fig 1.1B). The magnitude of the correlations for all gene pairs were relatively low with an average of  $r = 0.16$  compared to just cell cycle genes at  $r = 0.44$ . Assuming most genes are generally informative, one interpretation of the low correlations and heterogeneous

transcript distributions is that transcripts contain unique information. To test this hypothesis, we quantified the transcriptional information by performing PCA then calculating the differential entropy, a measure of information for continuous probability distributions, of the components (Equation 2, Fig 1.1C-E). Because each principal component is an independent, weighted sum of the row vectors of the data, we can approximate the differential entropy among orthogonal components assuming normality via the central limit theorem. Differential entropy across principal components does not measure the information in absolute terms but can describe how the information is distributed relative to the explained variance. We found that 6 principal components explain 75% of the variance, but only 15% of the gene entropy. The contrast between Fig 1.1C and 1.1D appears contradictory in that few orthogonal components explain most of the variance, yet entropy is steadily added across components with no obvious plateau. This analysis shows that simple measures such as explained variance that are often used for dimensionality reduction are not necessarily appropriate proxies of information content. Accounting for relevant, phenotypic information could help resolve discrepancies between explained variance and differential entropy. To estimate the signal entropy, i.e., information content in  $\text{Ca}^{2+}$  signaling, we took advantage of its dynamic patterns. Differential entropy of  $\text{Ca}^{2+}$  can be estimated using spectral entropy (Equation 1), a scale-invariant measure of information (Burg, 1975). The periodogram shows a continuum of signal frequencies with apparently low variance (Fig 1.1F). Signal entropy can be calculated using this distribution of frequencies, which we found to be 4.2 bits or ~18 signaling states. The mutual information between mRNA abundance and  $\text{Ca}^{2+}$  signaling is bounded by the distribution with the lowest entropy. Thus, 4.2 bits provides a likely upper bound to the true mutual information between transcripts and  $\text{Ca}^{2+}$  signals.

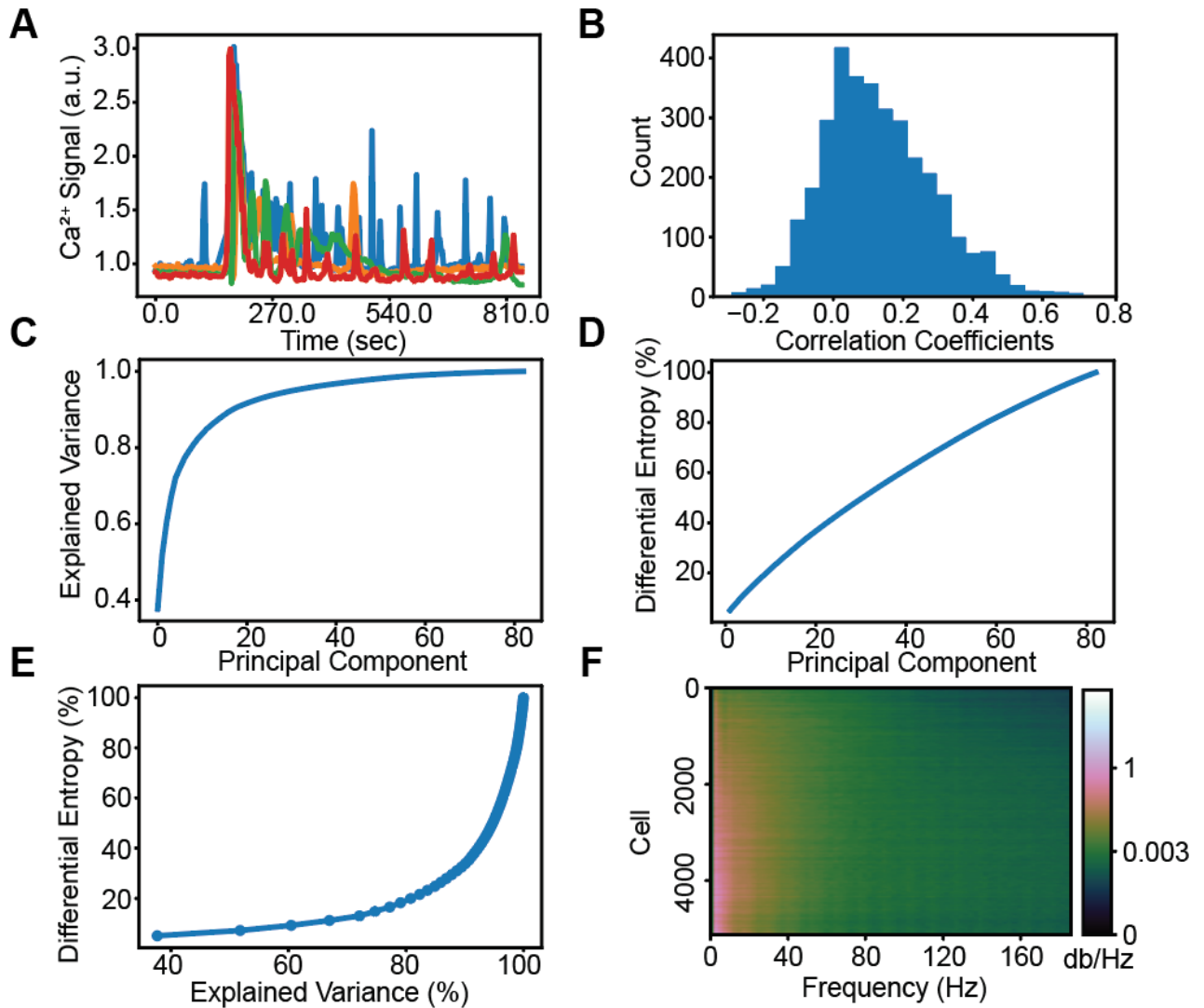


**Figure 1.1. Structure of Gene and  $\text{Ca}^{2+}$  Data.** A) Representative examples of  $\text{Ca}^{2+}$  dynamics of four cells in the dataset. B) A histogram of the pairwise gene correlation matrix which highlights the relatively low correlations. C) Explained variance of mRNA transcript counts from PCA. D) Differential entropy of transcripts estimated by PCA. E) Plot of explained variance (panel C) vs differential entropy (panel D) with an increasing number of principal components. Collectively, panels C-E show that most of the entropy comes from components that do not explain much of the variance. F) Dynamic  $\text{Ca}^{2+}$  signal periodogram (cropped to show only the lower wavelength, higher power frequencies).  $\text{Ca}^{2+}$  dynamic signals were found to contain a spectral entropy of 4.2 bits.

To quantify how useful phenotypic information is distributed across genes, we estimated mutual information between individual genes and  $\text{Ca}^{2+}$  signals (Fig 1.2A). To help choose hyperparameters and evaluate MINE's performance, we tested the model on multivariate gaussian distributions and found a mean residual of 0.37 bits with a Pearson correlation coefficient of 0.97 to the ground truth (Appendix Figure S2). Applied to the experimental data, we measured the total mutual information between all genes and  $\text{Ca}^{2+}$  at 2.5 +/- 0.4 bits. Most individual genes contain significant information about  $\text{Ca}^{2+}$  signals, an average of 0.7 bits, and the most informative gene accounts for 34% of the 4.2 bits of signal entropy. Cell cycle-associated genes were well distributed throughout the list, whereas genes coding for  $\text{Ca}^{2+}$  and/ or calmodulin-dependent proteins like *PPP3CA* and *CCDC47* were at the top of the list. If each gene contained completely unique information, then the sum of the phenotypic information in each gene should add up to the total of 2.5 +/- 0.4 bits. Interestingly, this sum is significantly larger than the total  $I(G; \text{Ca}^{2+})$ , indicating a high degree of redundancy (Fig 1.2B). The average mutual information between a single gene and  $\text{Ca}^{2+}$  signals is 0.7 bits, which is 17% of the signal entropy (Fig 1.2C). How the mutual information is shared across genes is not immediately clear. We further tested whether informative genes, i.e., genes that have high average pairwise mutual information to other genes, are also informative about  $\text{Ca}^{2+}$  dynamics (Fig 1.2D). Overall, genes that are more informative about  $\text{Ca}^{2+}$  signaling are also more informative about the expression of other genes. These genes that are highly informative about  $\text{Ca}^{2+}$  and many other transcripts may be interpreted as summary genes containing redundant, but distributed information. The second most informative single gene, *PPP1CA*, exemplifies this effect, as it codes for a subunit of PP1 that interacts with >200 regulatory proteins involved in a myriad of critical cell processes. Notably, the top two most informative genes, *PPP3CA* and *PPP1CA*, are both broadly connected phosphatases; kinases and phosphatases were consistently informative and concentrated towards the top of the list. However, from this analysis alone it is not clear how many genes contain redundant information and to what extent.

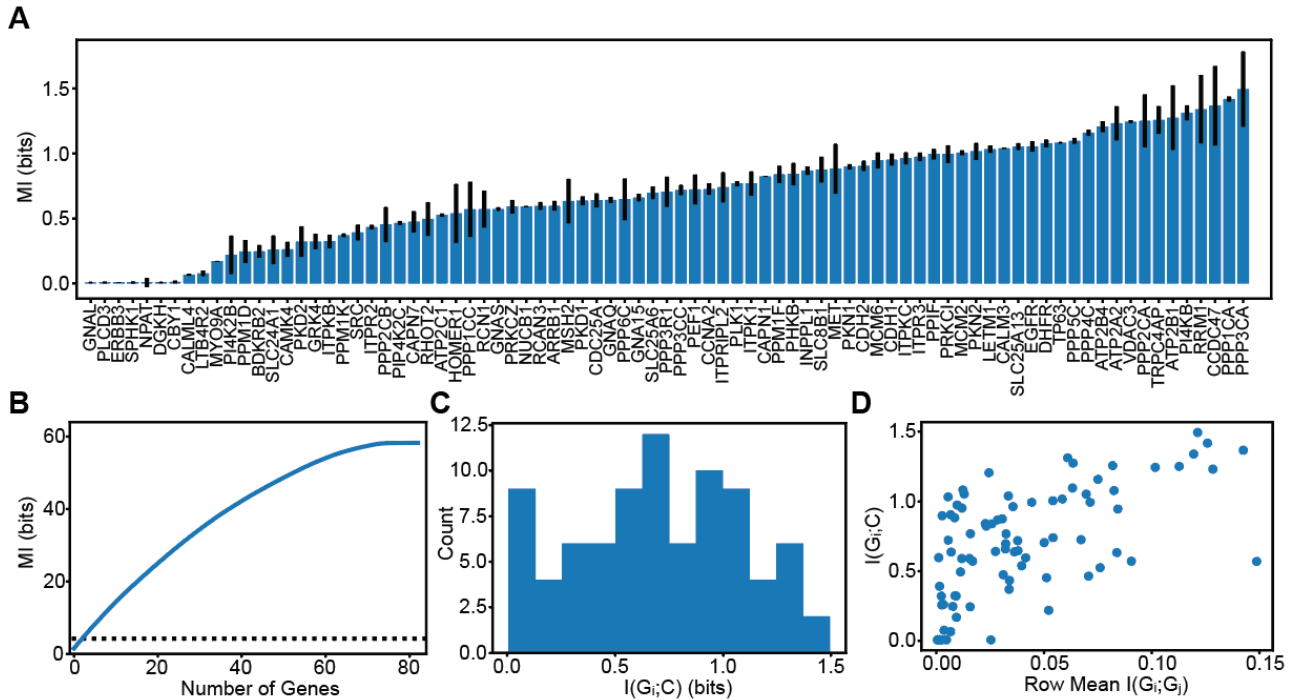


**Figure 1.2. Mutual Information Between Individual Genes and Ca<sup>2+</sup> Signals.** A)  $I(G_i;Ca^{2+})$  sorted from least to greatest, error bars are s.e. B) The blue line shows the cumulative sum of  $I(G_i;Ca^{2+})$  from (A) sorted from greatest to least, and individual genes appear to contain a lot of information (56 bits) about Ca<sup>2+</sup> signals. The black dashed line shows mutual information between all 83 genes and Ca<sup>2+</sup> dynamics estimated to be 2.5 bits. C) Histogram of (A) showing the mean  $I(G_i;Ca^{2+})$  is 0.7 bits. D)  $I(G_i;G_j)$  represents the pairwise mutual information between genes, the information that genes have about each other. This plot shows that genes that are more informative about other genes tend to be more informative about Ca<sup>2+</sup> dynamics.

To better understand how the superfluous information in Fig 1.2B is distributed among genes, we calculated the Synergy Redundancy Index (SRI) between gene pairs with respect to Ca<sup>2+</sup> (Dietterich *et al*, 2002; Schneidman *et al*, 2003).  $SRI(G_i, G_j | Ca^{2+})$  measures the information overlap between genes by subtracting  $I(G_i;Ca^{2+})$  and  $I(G_j;Ca^{2+})$  from  $I(\{G_i, G_j\};Ca^{2+})$ . A gene pair with negative SRI means that the sum of the mutual information between each gene and Ca<sup>2+</sup> was

greater than the gene pair, so the genes must contain some of the same information (redundant). A positive SRI indicates that there is more information about  $\text{Ca}^{2+}$  in the gene pair than in the sum of the individual genes (synergistic). An SRI of 0 describes a pair of genes that are either generally uninformative or are independent, containing unique and non-overlapping information about  $\text{Ca}^{2+}$ . Calculating SRI between all gene pairs reveals that most pairs are significantly redundant (Fig 1.3A, B). On average, gene pairs share 0.43 bits which accounts for 61% of the 0.7 bits of phenotypic information contained in the average individual gene. Further, the more informative a gene is about  $\text{Ca}^{2+}$ , the more redundant it is with other genes (Fig 1.3C). This finding supports that some genes aggregate information from many others and the more information a gene has, the more it shares. Consistent with findings in Fig 1.2A, phosphatases and kinases like *PPP3CA*, *PRKCI*, *PPP2CA*, *PI4KB*, and *PPP1CA* were among the most redundant. Interestingly, some genes are highly synergistic on average. One such synergistic gene is *PLCD3*, which appears to have no information about  $\text{Ca}^{2+}$  on its own, but suddenly becomes informative in gene pairs. *PLCD3* codes for an isoform of phospholipase C, a critical step in the  $\text{Ca}^{2+}$  in the signal transduction of extracellular ATP. It is surprising that *PLCD3* expression appears to contain little information about  $\text{Ca}^{2+}$  on its own considering its relevance to stimulus sensing, but this apparent paradox is reconciled by its high synergy. The most synergistic gene on average was *ATP2C1*, which codes for a calcium-transporting ATPase that couples ATP hydrolysis with  $\text{Ca}^{2+}$  transport into the Golgi lumen. Genes which are critical for modulating  $\text{Ca}^{2+}$  concentrations in the cytoplasm represent steps in linear processes, rather than cooperating with many other components to achieve their function. Generally, the most synergistic genes were not very informative on their own (Fig 1.2A) but became informative in a group of 2 (Fig 1.3C). The high degree of synergy suggests that these genes provide contextual or conditional information that is absent from most other genes, even genes that were independently informative. Most of the genes with near zero SRI were generally uninformative about signaling based on Fig 1.2A. Although, genes typically function



in larger sets beyond pairs, and a thorough understanding of transcriptional information requires evaluation of higher order interactions.

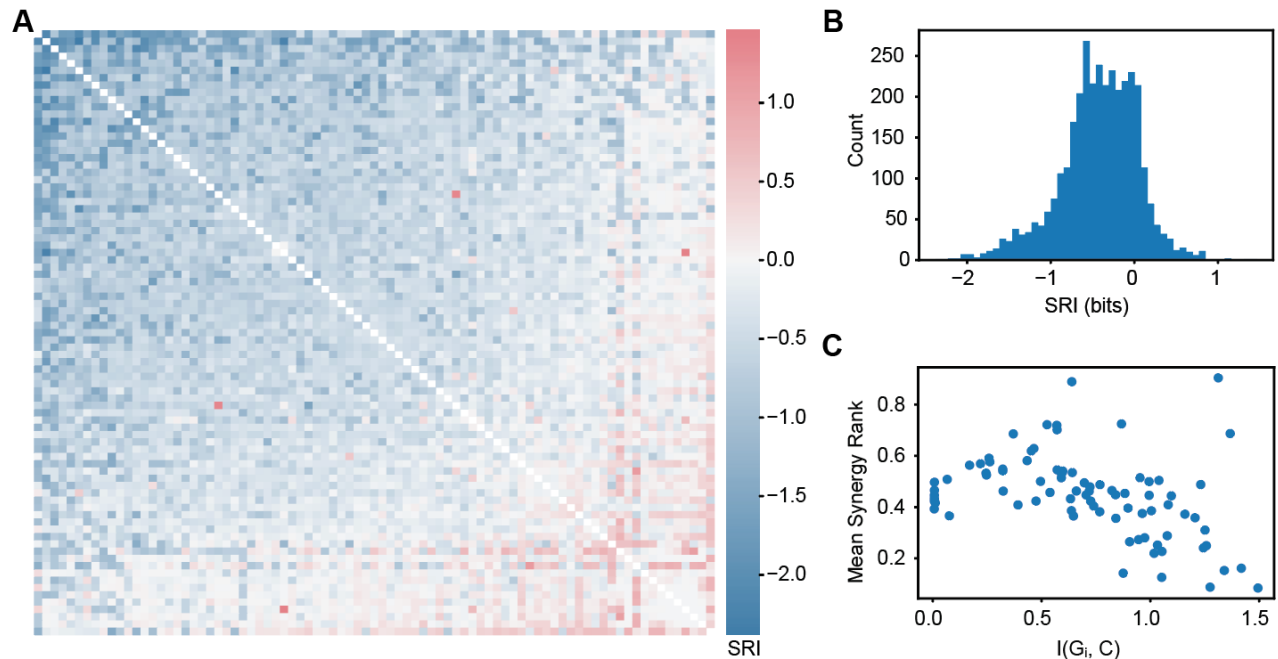


**Figure 1.3. Synergy and Redundancy of Gene Pairs with Respect to Ca<sup>2+</sup>.** A)  $SRI(G_i, G_j; Ca^{2+})$  sorted by average SRI. B) Histogram of SRI showing that most gene pairs are highly redundant with an average score of -0.43 bits. C) The mean rank of all synergistic pairs compared to the mutual information between that gene and Ca<sup>2+</sup> signals, (spearman  $r=0.5$ ,  $P<2e-6$ ), indicating that genes with more information about Ca<sup>2+</sup> are also more redundant.

To explore the mutual information between Ca<sup>2+</sup> and gene sets of various sizes, we tested various sets using gene annotations, a sequential search, and PCA. To quantify set level information at a functional level, we summarized pairwise SRIs based on gene annotations (Fig 1.4A). Calculating the mean SRI for combinations of annotations revealed how different functional gene sets contain phenotypic information. The Ca<sup>2+</sup>/ER annotation contains the most redundancies by a large margin, whereas the miscellaneous category “Other” is the most synergistic which can be explained by the functional diversity in this group. The Ca<sup>2+</sup>/ER annotation contains the genes

most relevant to the stimulus and appear to provide similar information. To understand how phenotypic information depends on gene set size, we calculated the mutual information between  $\text{Ca}^{2+}$  signals and gene sets of all sizes. Because testing all possible sets is prohibitively computationally expensive, we first sampled random sets of all possible sizes (4B). Each set size was sampled 4 times. For random sets, 53 genes contained 54% of the phenotypic information. To understand the upper and lower bounds on information in each set, we performed two directed heuristic searches. The directed searches first picked the most (least) informative gene, and then tested every possible addition to the set to add the member that contributed the most (least) information until the sets were of maximum size. The upper bound in green shows that the information quickly plateaus as the best 12 genes contain 54% of the phenotypic information, and all further additions contribute minimal additional information. Compared to random gene sets, using only the most informative combination of genes dramatically reduces the number of genes required to recapitulate most of the phenotypic information from 53 to 12. The lower bound in purple shows the unique information per gene given the set, sorted from least to greatest. Because the lower bound always adds the least informative and most redundant genes first, the last genes contain the most unique information. *PPP3CA* is the first gene added to the upper bound and the last gene to be added to the lower bound, which means it must have both the most absolute information and the most unique information. Interestingly, the growth of information in the least informative set was approximately linear, meaning that there is always some unique information in every gene. The slope of the lower bound is 0.03 bits, which represents the average unique information per gene.

Using the mean mutual information between a gene set and  $\text{Ca}^{2+}$ , we can also estimate the “redundancy explained” of all sets of genes of a given size according to Equation 5 (Fig 1.4C). We found that sets of only three genes explain 66% of the redundancy. Small gene sets contain much more redundant phenotypic information than larger gene sets. The point at which this curve begins to level off can be interpreted as a fundamental set size above which most phenotypic information

lies within the sets. We observe that small gene sets contain most of the information on  $\text{Ca}^{2+}$  dynamics suggesting that higher order interactions in larger sets are not required to capture the full dependency between mRNA abundance and  $\text{Ca}^{2+}$  dynamics.

Finally, we calculated the mutual information between transcript principal components and  $\text{Ca}^{2+}$  signals to compare with differential entropy (from Fig 1.1D) and understand how useful phenotypic information is distributed (Fig 1.4D). In agreement with Fig 1.4C, phenotypic information saturates quickly with only 3 principal components accounting for 74% of the 2.5 bits of mutual information between transcripts and signals. This result starkly contrasts with the differential entropy of gene principal components independent of  $\text{Ca}^{2+}$  signals which rises slowly and does not appear to plateau. By accounting for phenotypic information, far fewer orthogonal components are required to preserve the useful information. The difference between these curves indicates that focusing on phenotypic information may filter or compress transcriptional information.  $I(\text{PC};\text{Ca}^{2+})$  resembles the curve in Fig 1.1C, though still plateaus more quickly. These results confirm that phenotypic information is mostly explainable by a few components and higher order interactions do not significantly contribute.

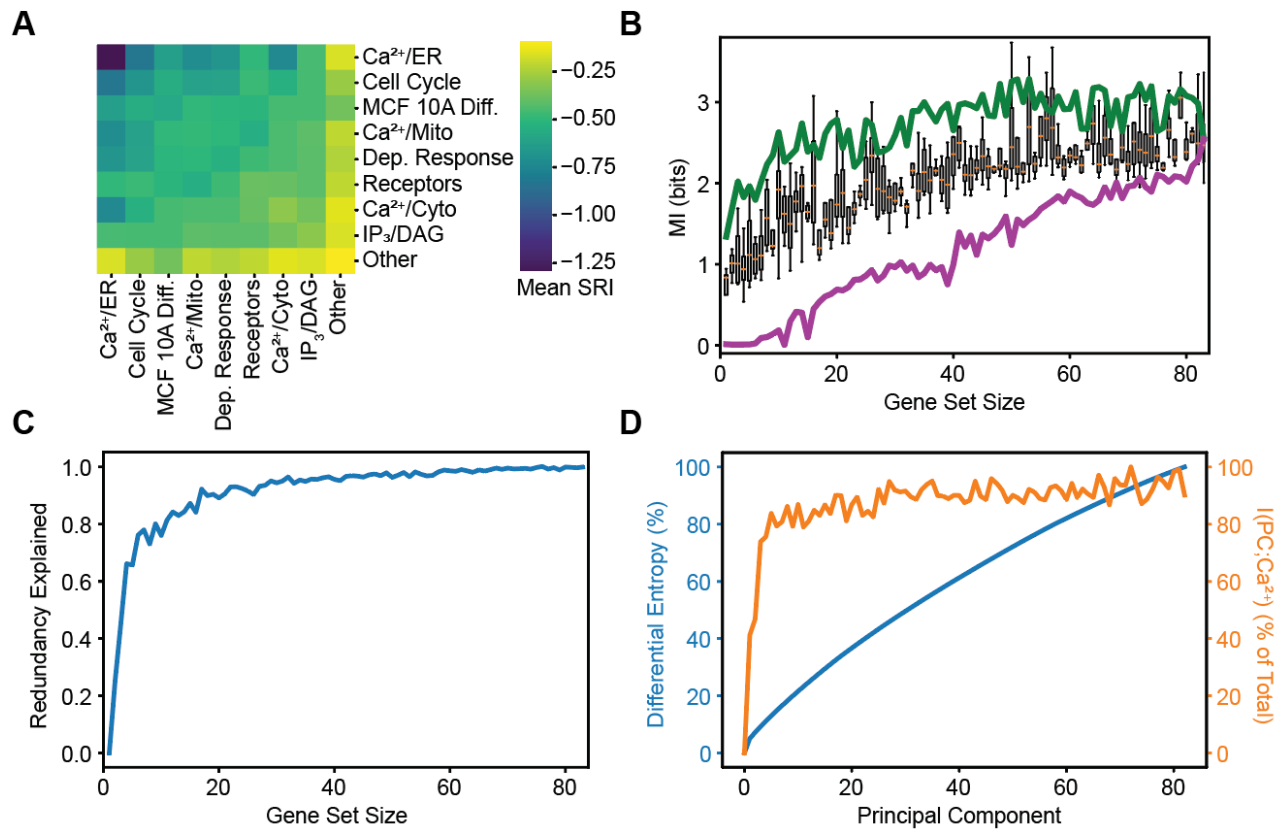


**Figure 1.4: Mutual Information Between Gene Sets and Ca<sup>2+</sup> Signals.** A) Mean pairwise SRI from Figure 1.3 for sets based on annotation. MCF 10A differentiation and Ca<sup>2+</sup> dependent response are abbreviated. B) Gene sets of various sizes were constructed using three different strategies: an upper bound (green) that always adds the most informative gene to the set given the genes already included, random strategy (boxes) that samples random sets of genes, and a lower bound (purple) that always adds the least informative gene to the set given the genes already included. C) Blue line shows total information using the expected value of  $I(\{G_0, \dots, G_n\}; Ca^{2+})$ . D) A y-y plot of gene differential entropy in blue (same as Figure 1.1D) and the mutual information between gene principal components and Ca<sup>2+</sup> in orange. Both values are normalized by their respective max values.

## Discussion

The complexity of biological regulation is staggering. While many details about biological networks are known, the gaps in our knowledge make some simple questions very challenging to answer. For example, to what degree does abundance of one set of molecules matter? Specifically, does the abundance of mRNAs matter for the regulation of complex cellular phenotypes such as signaling response to a ligand? Here we provide a framework for answering such questions through the combination of paired single cell data and application of recent advances at the interface between machine learning and information theory (Belghazi *et al*, 2018). Applying a recently developed framework for mutual information estimation to single cell data of multiplexed mRNA levels paired with live cell imaging allowed us to quantify the strength of the causal connection between mRNAs and  $\text{Ca}^{2+}$  signaling. We found that approximately 60% of  $\text{Ca}^{2+}$  signal information exists in transcript counts, which is 2.5 (+/- 0.4) bits. Furthermore, the framework we developed provides key information about information synergy and redundancy, can be used to quantify the joint information in sets of genes, and reveals how overall dependency changes with the size of the set. On average, genes were found to contain 61% redundant information with each other, though nearly all genes contained some unique information. Genes that appeared to contain little phenotypic information individually were in fact the most synergistic and became informative in pairs. The unique information present in gene sets is best visualized in Fig. 4B, which illustrates the difference in information among the most, least, and average set. In the best case, only 12 genes contain 54% of signal information, which is significantly fewer than an equally informative 53 random genes. While all genes contain unique information, some sets are still significantly more informative than others likely due to their role in the signaling network. Decomposition by principal components (Fig. 4D) revealed a rapid plateau in phenotypic information, starkly contrasting the increasing growth in differential entropy. These results demonstrate the utility of information theoretic analysis in quantifying the phenotypic information of mRNA abundance.

The framework we propose is very general and can be applied to any two “slices” within a complex biological regulatory network. Our numerical experiments (Supplementary Material) demonstrate that with minor adaptations for bias removal, MINE can robustly estimate mutual information between two high dimensional vectors containing 100+ features. The generalizability of this framework provides a new tool to put weights and interpretable numbers on different “arrows” within complex biological regulatory networks. Importantly, such “arrows” do not necessarily represent direct mechanistic steps. There are numerous reactions that occur post transcriptionally to determine  $\text{Ca}^{2+}$  signaling responses. Yet, using MINE we were able to infer the individual contribution of each gene in controlling the emergent phenotypes. Furthermore, using pairs of genes and estimation of the effect of gene set size, we determined how information between multiple mRNA types is integrated. This inference showed that despite the information having to propagate through multiple layers of regulation, it still shows significant dependency. Even though correlations between mRNA and protein levels are generally low, a substantial amount of phenotypically relevant information is still preserved in the transcriptome. Our results support the use of mRNA measurements to infer and predict useful phenotypic characteristics of cell populations. One interpretation of the 2.5 (+/- 0.4) bits of mutual information is that transcripts can differentiate approximately 6 distinct states of  $\text{Ca}^{2+}$  signaling dynamics. An important feature of our analysis is that all inference was done relying on natural heterogeneity without any experimental perturbation to gene expression circumventing compensation and non-linear dependencies that are common pitfalls of perturbation analysis (Welf & Danuser 2014).

While the framework we propose is very general, our findings are systems specific and will change depending on the set of genes and measured phenotypes. Here we focused on  $\text{Ca}^{2+}$  signaling in response to activation of GPCR in a clonal population of MCF 10A cells. In previous work, we estimated that a cellular population is composed of multiple subtypes (Yao *et al*, 2016) and have shown that mRNA variability is dominated by cell state differences with a minor contribution from transcriptional bursting (Foreman & Wollman, 2020). Our current finding that 60%

of information in the emerging  $\text{Ca}^{2+}$  signaling phenotypes can be attributed to cellular transcriptional state largely agrees with these previous findings. It is likely that in other systems, decomposition of information content will differ from the 60% transcriptional and 40% post transcriptional measured here. For example, broad phenotypes such as cell type classification that often correspond to larger and highly patterned transcriptional differences will likely show higher levels of transcriptional dependency. Additionally, it is possible that the full transcriptome may contain more phenotypic information than is found in just the 83 genes measured in this study. While only 12 genes accounted for most of the shared information, the apparent plateau and informational redundancy may result from the strong functional relationships and dependencies in the selected gene set. Including significantly more genes related to other cellular processes may provide more information about the observed phenotype by better defining the transcriptional state or revealing indirect dependencies to other cellular processes.

Our approach has several limitations, experimental and computational, that will need to be addressed in future work. Experimentally, gene selection, i.e., the expression of which genes are measured, is limited due to gene length, specific sequence, and other experimental constraints that are continuously improving. Furthermore, the approach could be applied to tissue samples with much higher population diversity where the relationship between transcripts and phenotype is more relevant. Computationally, because of stochastic gradient ascent, the model's estimates are somewhat noisy and required multiple replicates. Additionally, we were limited to exploring the effect of set sizes with search strategies and only exhaustively examined pairwise dependencies because the model was computationally expensive to run. None of the search strategies are guaranteed to find the truly most or least informative set because doing so would require a prohibitively time-consuming, exhaustive search. Despite these limitations, MINE was able to provide an interpretable and scalable quantification of dependency between transcript sets and  $\text{Ca}^{2+}$  signaling.

Recent advances in single cell technologies are making high-dimensional, multimodal measurements feasible. Statistical descriptions of complex phenotypes will become increasingly useful as single cell experiments generate more multimodal and multiomic data. Integrating multiple different data types is still a challenge in the field, and this work represents a new approach to synthesize statistical descriptions of high-dimensional, multimodal data that does not make any assumptions about the underlying functional relationships. This unbiased approach will enable a deeper understanding of complex, multidimensional data by quantifying the dependency between any single cell phenomena.

## Methods

*Data Selection.* Data collection is described in previous work (Foreman & Wollman, 2020). Of the 336 genes measured, 150 genes were measurably expressed and the top 83 were chosen by the highest magnitude z scores from multiple linear regression.

*Preprocessing.* Transcript counts from the 83 genes and 314 timepoints of  $\text{Ca}^{2+}$  signals were independently z-score normalized. Normalization was applied to the entire matrix of all cells for each data type (e.g., 5128x83 for transcripts) and not to individual columns, preserving relative magnitude across genes and timepoints.

*Spectral Entropy.* Spectral entropy of a signal is defined as the Shannon entropy ( $H$ ) of the probability distribution of the normalized power spectral density ( $P(f)$ ), calculated here using the Fourier transform. Although the calculation requires a sampling frequency ( $f_s$ ), the result does not change above a sufficiently large value.

$$H(f_s) = - \sum_{f=1}^{f_s/2} P(f) \log_2 P(f)$$



(1)

*Differential Entropy:* Differential entropy was calculated via the determinant of the covariance matrix of the PCA-transformed data. This approach was used to estimate the entropy of the mRNA transcript counts.

$$\frac{n}{2} + \frac{n \log_2 2\pi}{2} + \det \Sigma_{PC} \quad (2)$$

$n$  = number of principal components,  $\Sigma$  = the covariance matrix,  $PC$  = PCA-transformed data for a given  $n$

*MINE.* Hyperparameters were chosen by fitting analytically tractable data from an additive white gaussian noise model of the data across a range of strengths of dependence (Appendix Figure S1). Additional bias correction was implemented by fitting  $I_{obs}(t) = I_{true}(1 - a) * e^{-b*t} + ct$ , where  $I_{true}$ ,  $a$ ,  $b$ , and  $c$  are fitting parameters and  $t$  is the number of iterations (Appendix Figure S2). Convergence tests were performed on the real data by comparing the residuals of the bias correction fit. The chosen hyperparameters of 600 hidden units and a learning rate = 3e-4 resulted in the highest yield, i.e., fewest failed fits.

*Synergy Redundancy Index (SRI).* The Synergy Redundancy Index was developed to evaluate information about a stimulus shared among a small population of cells (Dietterich *et al*, 2002). Equation 3 describes the calculation, which involves comparing pairwise and individual mutual information between genes and  $Ca^{2+}$  signals.

$$SRI(G_i, G_j | Ca^{2+}) = I(G_i, G_j; Ca^{2+}) - I(G_i; Ca^{2+}) - I(G_j; Ca^{2+}) \quad (3)$$

First, the mutual information between each unique pair of genes and  $Ca^{2+}$  were estimated,  $I(G_i, G_j; Ca^{2+})$ . Then  $I(G_i; Ca^{2+})$  was calculated, and Equation 3 was calculated for all genes.

*Redundancy Explained.* This metric represents the amount of extra information assuming no redundancy between elements. Equation 4 first calculates an expected value by taking the mean of sampled gene sets of size  $k$ . The expected value is multiplied by the number of possible sets then divided the number of times an individual gene appears in all sets to calculate the nonredundant information (NRI) as if all individual sets contain unique information:

$$NRI = \frac{\mathbb{E}[I(\{G_1, \dots, G_k\}; Ca^{2+})] \binom{n}{k}}{\binom{n-1}{k-1}} = \mathbb{E}[I(\{G_1, \dots, G_k\}; Ca^{2+})] \frac{n}{k} \quad (4)$$

$k$  = set size,  $n$  = total number of genes

From Equation 4, we can calculate the fraction of purely redundant information for a set of size  $k$  out of the maximum, which is the NRI at  $k=1$  minus the full mutual information. The Redundancy Explained (RE) is calculated as follows:

$$RE = 1 - \frac{NRI_k - I(G; Ca^{2+})}{NRI_1 - I(G; Ca^{2+})} \quad (5)$$

**Acknowledgments:** We thank Robert Foreman for significant analytical and conceptual contributions, as well as Alon Oyler-Yaniv for suggesting spectral entropy to quantify  $Ca^{2+}$  signal information. We gratefully acknowledge the support of NVIDIA Corporation for donation of the two Titan V GPUs used for this research.

## References

Adelaja A, Taylor B, Sheu KM, Liu Y, Luecke S & Hoffmann A (2021) Six distinct NF $\kappa$ B signaling codons convey discrete information to distinguish stimuli and enable appropriate macrophage responses. *Immunity* 54: 916–930.e7

- Alves M, Beamer E & Engel T (2018) The Metabotropic Purinergic P2Y Receptor Family as Novel Drug Target in Epilepsy. *Front Pharmacol* 9: 193
- Azeloglu EU & Iyengar R (2015) Signaling networks: information flow, computation, and decision making. *Cold Spring Harb Perspect Biol* 7: a005934
- Bagur R & Hajnóczky G (2017) Intracellular Ca<sup>2+</sup> Sensing: Its Role in Calcium Homeostasis and Signaling. *Mol Cell* 66: 780–788
- Balázsi G, van Oudenaarden A & Collins JJ (2011) Cellular decision making and biological noise: from microbes to mammals. *Cell* 144: 910–925
- Belghazi MI, Baratin A, Rajeswar S, Ozair S, Bengio Y, Courville A & Devon Hjelm R (2018) MINE: Mutual Information Neural Estimation. *arXiv [csLG]*
- Brennan MD, Cheong R & Levchenko A (2012) Systems biology. How information theory handles cell signaling and uncertainty. *Science* 338: 334–335
- Burg JP (1975) Stanford University.
- Cheong R, Rhee A, Wang CJ, Nemenman I & Levchenko A (2011) Information transduction capacity of noisy biochemical signaling networks. *Science* 334: 354–358
- Darmanis S, Gallant CJ, Marinescu VD, Niklasson M, Segerman A, Flamourakis G, Fredriksson S, Assarsson E, Lundberg M, Nelander S, *et al* (2016) Simultaneous Multiplexed Measurement of RNA and Proteins in Single Cells. *Cell Rep* 14: 380–389
- Dietterich TG, Becker S & Ghahramani Z (2002) Advances in Neural Information Processing Systems: Proceedings of the 2001 Conference MIT Press
- El-Samad H (2021) Biological feedback control-Respect the loops. *Cell Syst* 12: 477–487

- Emert BL, Cote CJ, Torre EA, Dardani IP, Jiang CL, Jain N, Shaffer SM & Raj A (2021) Variability within rare cell states enables multiple paths toward drug resistance. *Nat Biotechnol* 39: 865–876
- Fang R, Preissl S, Li Y, Hou X, Lucero J, Wang X, Motamedi A, Shiau AK, Zhou X, Xie F, *et al* (2021) Comprehensive analysis of single cell ATAC-seq data with SnapATAC. *Nat Commun* 12: 1337
- Foreman R & Wollman R (2020) Mammalian gene expression variability is explained by underlying cell state. *Mol Syst Biol* 16: e9146
- Gayoso A, Steier Z, Lopez R, Regier J, Nazor KL, Streets A & Yosef N (2021) Joint probabilistic modeling of single-cell multi-omic data with totalVI. *Nat Methods* 18: 272–282
- Genshaft AS, Ziegler CGK, Tzouanas CN, Mead BE, Jaeger AM, Navia AW, King RP, Mana MD, Huang S, Mitsialis V, *et al* (2021) Live cell tagging tracking and isolation for spatial transcriptomics using photoactivatable cell dyes. *Nat Commun* 12: 1–15
- Gong H, Wang X, Liu B, Boutet S, Holcomb I, Dakshinamoorthy G, Ooi A, Sanada C, Sun G & Ramakrishnan R (2017) Single-cell protein-mRNA correlation analysis enabled by multiplexed dual-analyte co-detection. *Sci Rep* 7: 2776
- Hafner A, Stewart-Ornstein J, Purvis JE, Forrester WC, Bulyk ML & Lahav G (2017) p53 pulses lead to distinct patterns of gene expression albeit similar DNA-binding dynamics. *Nat Struct Mol Biol* 24: 840–847
- Jacques M-A, Dobrzyński M, Gagliardi PA, Sznitman R & Pertz O (2021) CODEX, a neural network approach to explore signaling dynamics landscapes. *Mol Syst Biol* 17: e10026

- Kinnunen PC, Luker KE, Luker GD & Linderman JJ (2021) Computational methods for characterizing and learning from heterogeneous cell signaling data. *Current Opinion in Systems Biology* 26: 98–108
- Lane K, Van Valen D, DeFelice MM, Macklin DN, Kudo T, Jaimovich A, Carr A, Meyer T, Pe'er D, Boutet SC, *et al* (2017) Measuring Signaling and RNA-Seq in the Same Cell Links Gene Expression to Dynamic Patterns of NF- $\kappa$ B Activation. *Cell Syst* 4: 458–469.e5
- Lee J, Hyeon DY & Hwang D (2020) Single-cell multiomics: technologies and data analysis methods. *Exp Mol Med* 52: 1428–1442
- Liu M, Yang B, Hu M, Radda JSD, Chen Y, Jin S, Cheng Y & Wang S (2021) Chromatin tracing and multiplexed imaging of nucleome architectures (MINA) and RNAs in single mammalian cells and tissue. *Nat Protoc* 16: 2667–2697
- Liu Y, Beyer A & Aebersold R (2016) On the Dependency of Cellular Protein Levels on mRNA Abundance. *Cell* 165: 535–550
- Macaulay IC, Ponting CP & Voet T (2017) Single-Cell Multiomics: Multiple Measurements from Single Cells. *Trends Genet* 33: 155–168
- Mair F, Erickson JR, Voillet V, Simoni Y, Bi T, Tyznik AJ, Martin J, Gottardo R, Newell EW & Prlic M (2020) A Targeted Multi-omic Analysis Approach Measures Protein Expression and Low-Abundance Transcripts on the Single-Cell Level. *Cell Rep* 31: 107499
- Moffitt JR, Hao J, Wang G, Chen KH, Babcock HP & Zhuang X (2016) High-throughput single-cell gene expression profiling with multiplexed error-robust fluorescence in situ hybridization. *Proc Natl Acad Sci U S A* 113: 11046–11051

- Myers PJ, Lee SH & Lazzara MJ (2021) Mechanistic and data-driven models of cell signaling: Tools for fundamental discovery and rational design of therapy. *Current Opinion in Systems Biology* 28: 100349
- Nelson DE, Ihekwaba AEC, Elliott M, Johnson JR, Gibney CA, Foreman BE, Nelson G, See V, Horton CA, Spiller DG, *et al* (2004) Oscillations in NF-kappaB signaling control the dynamics of gene expression. *Science* 306: 704–708
- Park S & Pardalos PM (2021) Deep Data Density Estimation through Donsker-Varadhan Representation. *arXiv [csLG]*
- Perkins TJ & Swain PS (2009) Strategies for cellular decision-making. *Mol Syst Biol* 5: 326
- Purvis JE & Lahav G (2013) Encoding and decoding cellular information through signaling dynamics. *Cell* 152: 945–956
- Putney JW (2012) Calcium signaling: deciphering the calcium-NFAT pathway. *Curr Biol* 22: R87–9
- Schneidman E, Bialek W & Berry MJ 2nd (2003) Synergy, redundancy, and independence in population codes. *J Neurosci* 23: 11539–11553
- Schulz D, Zanotelli VRT, Fischer JR, Schapiro D, Engler S, Lun X-K, Jackson HW & Bodenmiller B (2018) Simultaneous Multiplexed Imaging of mRNA and Proteins with Subcellular Resolution in Breast Cancer Tissue Samples by Mass Cytometry. *Cell Syst* 6: 25–36.e5
- Selimkhanov J, Taylor B, Yao J, Pilko A, Albeck J, Hoffmann A, Tsimring L & Wollman R (2014) Systems biology. Accurate information transmission through dynamic biochemical signaling networks. *Science* 346: 1370–1373

Shaffer SM, Emert BL, Reyes Hueros RA, Cote C, Harmange G, Schaff DL, Sizemore AE, Gupte R, Torre

E, Singh A, *et al* (2020) Memory Sequencing Reveals Heritable Single-Cell Gene Expression Programs Associated with Distinct Cellular Behaviors. *Cell* 182: 947–959.e17

Spencer SL, Gaudet S, Albeck JG, Burke JM & Sorger PK (2009) Non-genetic origins of cell-to-cell variability in TRAIL-induced apoptosis. *Nature* 459: 428–432

Stoeckius M, Hafemeister C, Stephenson W, Houck-Loomis B, Chattopadhyay PK, Swerdlow H, Satija R & Smibert P (2017) Simultaneous epitope and transcriptome measurement in single cells. *Nat Methods* 14: 865–868

Subramanian I, Verma S, Kumar S, Jere A & Anamika K (2020) Multi-omics Data Integration, Interpretation, and Its Application. *Bioinform Biol Insights* 14: 1177932219899051

Taniguchi Y, Choi PJ, Li G-W, Chen H, Babu M, Hearn J, Emili A & Xie XS (2010) Quantifying E. coli proteome and transcriptome with single-molecule sensitivity in single cells. *Science* 329: 533–538

Tostevin F & ten Wolde PR (2010) Mutual information in time-varying biochemical systems. *Phys Rev E Stat Nonlin Soft Matter Phys* 81: 061917

Uda S, Saito TH, Kudo T, Kokaji T, Tsuchiya T, Kubota H, Komori Y, Ozaki Y-I & Kuroda S (2013) Robustness and compensation of information transmission of signaling pathways. *Science* 341: 558–561

Wang G, Moffitt JR & Zhuang X (2018) Multiplexed imaging of high-density libraries of RNAs with MERFISH and expansion microscopy. *Sci Rep* 8: 4847

Welch JD, Kozareva V, Ferreira A, Vanderburg C, Martin C & Macosko EZ (2019) Single-Cell Multi-omic

Integration Compares and Contrasts Features of Brain Cell Identity. *Cell* 177: 1873–1887.e17

Welf ES, Danuser G. Using fluctuation analysis to establish causal relations between cellular events without experimental perturbation. *Biophys J*. 2014;107(11):2492-2498.

Wong VC, Mathew S, Ramji R, Gaudet S & Miller-Jensen K (2019) Fold-Change Detection of NF- $\kappa$ B at Target Genes with Different Transcript Outputs. *Biophys J* 116: 709–724

Yao J, Pilko A & Wollman R (2016) Distinct cellular states determine calcium signaling response. *Mol Syst Biol* 12: 894

Zhang M, Eichhorn SW, Zingg B, Yao Z, Cotter K, Zeng H, Dong H & Zhuang X (2021) Spatially resolved cell atlas of the mouse primary motor cortex by MERFISH. *Nature* 598: 137–143

Zhang Q, Gupta S, Schipper DL, Kowalczyk GJ, Mancini AE, Faeder JR & Lee REC (2017) NF- $\kappa$ B Dynamics Discriminate between TNF Doses in Single Cells. *Cell Syst* 5: 638–645.e5

Zuo C & Chen L (2021) Deep-joint-learning analysis model of single cell transcriptome and open chromatin accessibility data. *Brief Bioinform* 22



## CHAPTER 2

### Predicting Death Decisions from Signaling Dynamics

#### Abstract

Rapid death of infected cells is an important antiviral strategy. However, fast decisions that are based on limited evidence can be erroneous and cause unnecessary cell death and subsequent tissue damage. How cells optimize their death decision making strategy to maximize both speed and accuracy is unclear. In this work, I connect transcriptional activity and receptor complexes to this death decision. I show that tumor necrosis factor primes cells for apoptosis by assembling a receptor complex that requires active transcription to delay the death decision. Further, the caspase 8 activity immediately downstream of this receptor complex is strongly predictive of cell death many hours before the decision appears irreversible.

#### Introduction

Rapid detection of viral infection is needed to minimize spread and associated damage. At the same time, evolutionary pressures constantly enhance the arsenal of strategies that viruses use to evade and manipulate host detection (Duggal *et al*, 2012; Elde *et al*, 2009). The adversarial co-evolution between host detection and viral avoidance creates a challenging and time-dependent classification problem for host cells that likely operate close to the detection limits imposed by the inherent stochasticity of biochemical reactions. Rapid decision making at the noise limit is likely to result in false-positive classification i.e., a decision that a virus is there when it is not, followed by unnecessary cell death and bystander tissue damage. The timing and cellular processes underlying this decision has not been thoroughly explored.

The initial detection of viral invasion in a tissue is accomplished by macrophages and other innate immune sentinels (Murray *et al*, 2011). These specialized cells secrete cytokines and other

inflammatory mediators to alert nearby cells of invading pathogens. Alerted cells then execute diverse strategies to prevent viral spread including restriction of viral entry, direct inhibition of viral gene expression, prevention of viral genome replication, prevention of viral egress, and death of infected cells (Fensterl *et al*, 2015; Barber *et al*, 2001). These defense mechanisms are activated in an inducible manner as they have the potential to interfere with normal host cell physiology (Kash *et al*, 2006; Baskin *et al*, 2009; Cillóniz *et al*, 2009; Subramanian *et al*, 2018). We focused on Tumor Necrosis Factor (TNF) because it is an important antiviral cytokine (Benedict *et al*, 2003), yet can also cause significant damage to healthy host tissues due to its role regulating cell death pathways (Brenner *et al*, 2015). This relationship is exemplified by the observation that TNF-blocking drugs have shown remarkable success for treatment of autoimmune disorders, yet also increase susceptibility to certain pathogens (Croft *et al*, 2013). Further, excessive production of TNF has been implicated as an important driver of cell death and tissue destruction during infection with hyper-virulent virus strains such as the H5N1 and 1918 pandemic influenza subtypes (Kash *et al*, 2006; Baskin *et al*, 2009; Cillóniz *et al*, 2009).

While TNF represents a potentiating factor, capable of inducing assembly of various decision-making complexes, the deciding factor that explains the acceleration of decision speed is yet unknown. Understanding the decision dynamics at a single cell level would provide significant insights into host viral defenses and extend the applicability of decision theory to single cells. Most importantly, identification of the decision point could inform new antiviral therapies that sensitize cells to the virus early in the infection.

In this work, I use immunofluorescence, live-cell imaging, and logistic regression to connect an emerging, phenotypic decision with transcriptional activity and information at the level of protein activity. Using a sensitive, proximity-based immunofluorescence assay, I detected the presence of the death-inducing signaling complex (DISC) which triggers caspase 8 activity as a precursor to

apoptosis. Next, I showed that the timing of the death decision depends on transcriptional activity. Finally, I trained a classifier using logistic regression to predict death from caspase 8 activity.

## Results

To help identify relevant mechanisms of cell death, I measured how much TNF-induced decision speed depends on active transcription. Co-treatment with TNF and Actinomycin-D showed a dramatic decrease in time-to-death which was not observed in cells treated with either chemical alone (Fig 2.1A). This synergy outpaced even the TNF+virus condition (Oyler-Yaniv *et al*, 2021) and implicated active transcription in delaying the death decision. Further experiments showed that death by TNF alone was occurring by caspase 8-dependent apoptosis using caspase inhibitors (Oyler-Yaniv *et al*, 2021), which occurs when DISC transitions from signaling (complex 1) to apoptosis (complex 2). To confirm the sustained presence of DISC, I used a dual antibody proximity ligation assay (Duolink PLA) to probe for DISC in single cells. DISC was found with significantly higher abundance in TNF-treated cells as long as 48 hours post-treatment (Fig 2.1B, C). Long term presence of DISC and associated transcription can continuously upregulate inhibitors of DISC-mediated apoptosis (Fig 2.1D).

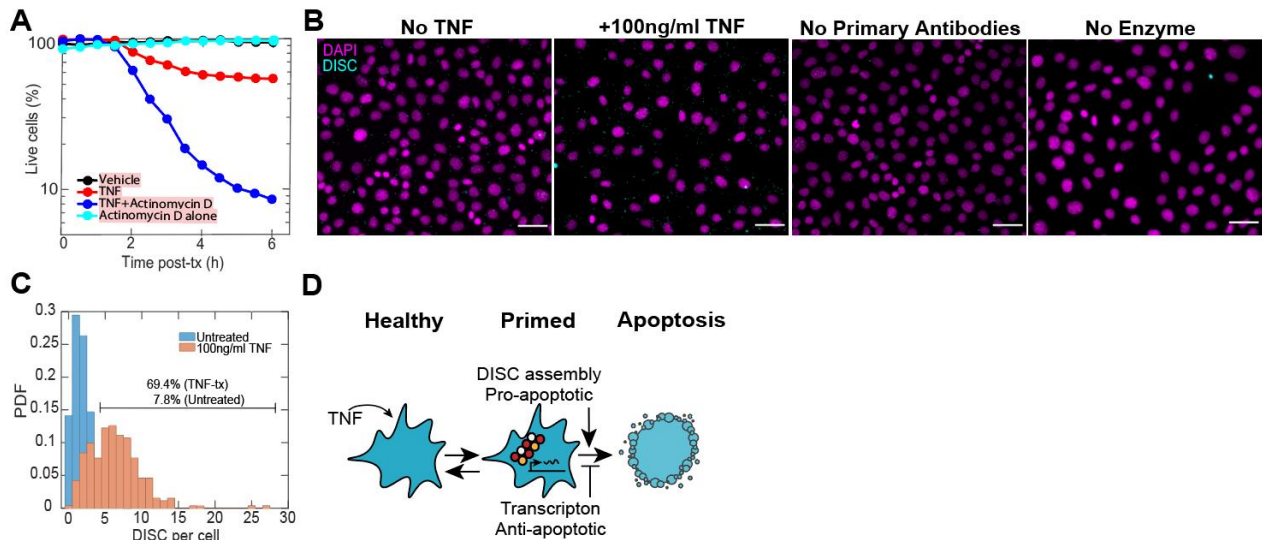


**Figure 2.1. DISC Connects Transcription and Death Decision Timing.** A) Actinomycin D and TNF synergistically speed up the death decision, indicating dependence on short-term

transcriptional activity. B) Images of DISCs forming in response to TNF treatment, all images were taken at 20x. The TNF treatment shows lower cell density to cell death. C) Histograms showing the increased DISC count per cell due to TNF treatment. D) A conceptual model of TNF priming, proapoptotic (DISC) and antiapoptotic (transcription) factors controlling the death decision speed.

To help determine when the death decision is irreversibly made, I used a machine learning approach to predict the probability of death from caspase 8 activity time series data. 3T3 cells with a caspase 8 FRET biosensor, which is activated upon cleavage, were stimulated with TNF and continuously imaged (Oyler-Yaniv *et al*, 2021). Death decision time was determined using a peak finding algorithm applied to the full signal and confirmed with a Sytox death stain (Fig 2.2A). To determine the upper bound on predictability, I first trained a recurrent neural network classifier with an attention layer (a matrix of timepoint importance learned by the model) on the signal trajectories. The model performed well on the subsets of the data with the largest sample size with time from death between 1 and 10 hours. Analyzing the attention layer indicated the most relevant features of the signal were the integral and max fold change, which are also common features in cell signal analysis. Reducing the data to these features allowed use of logistic regression, a simpler technique that would generalize better to low sample sizes and shorter signals. Logistic regression on these features performed about as well as the recurrent neural network on cells that dies within 1-10 hours of TNF stimulation and significantly outperformed outside this range as well. The logistic regression model performed better than random up to 29 hours ahead of detectable cell death (Fig 2.2B). Prediction ability was expectedly highest closest to cell death. These results indicate early caspase activity is strongly predictive of death, though the process is not fully deterministic.

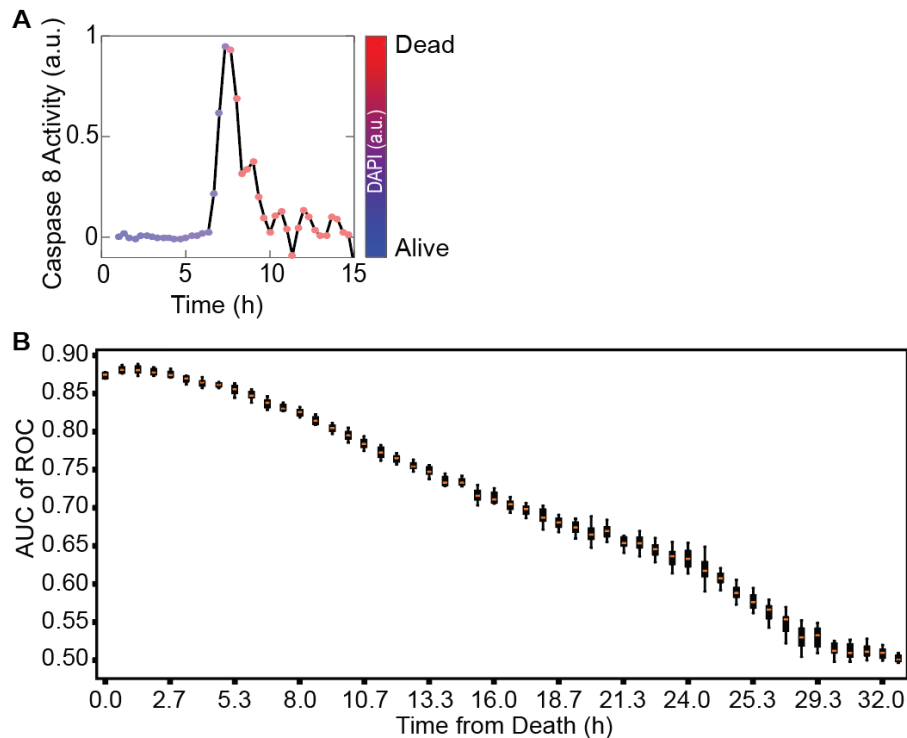


**Figure 2.2. Predicting Death from Caspase 8 Activity Over Time.** A) Caspase 8 activity in a 3T3 cell after TNF treatment using a FRET biosensor. B) Area under the curve of the receiver-operator characteristic for a cell death classifier using logistic regression.

## Discussion

In this chapter, I used live cell timelapse microscopy, machine learning, and immunofluorescence to investigate apoptotic decision dynamics in the context of an immune response. I found that TNF primes 3T3 cells for death by inducing the formation of DISCs. When TNF and a general transcriptional inhibitor, Actinomycin D were administered together, apoptosis occurred at a significantly faster rate than in either condition alone. The combined effect of both treatments supports that DISCs require transcriptional activity to delay the death decision. Furthermore, I analyzed caspase 8 activity from a FRET reporter using logistic regression to demonstrate that death is predictable in most cells several hours prior to membrane permeabilization and effector caspase activity. This predictability indicates that the decision is determined early on for many cells and supports the role of the DISC in triggering an irreversible amount of caspase 8 activity.

Although these results do not pinpoint the source of variability in decision speeds or the molecular mechanism, the continuous degradation in prediction performance is still informative about decision dynamics. TNF cannot directly induce death and must involve some intermediate deciding factor that varies across cells. The lack of a steep drop-off in prediction performance is inconsistent with graded variability that may emerge from simple thresholds (e.g., presence or absence of DISCs or a single transcript). Instead, it supports a drift-diffusion model of decision dynamics where cells pass some decision threshold that appears to be revealed in the caspase 8 dynamics. However, the deciding factor could be upstream of caspase 8 activity as indicated by the Actinomycin D experiments. One possible model is that the rate of production of some short-lived anti-apoptotic protein functions as the decision clock, with a functional timer even in absence of virus. Future experiments testing a broader array of specific inhibitors and or loss-of-function studies could reveal the decision factor, representing a focal point for cellular antiviral strategies.

## **Materials and Methods**

### *Cell Culture*

Mouse 3T3 fibroblasts were cultured in DMEM supplemented with 10% newborn calf serum (NBCS), 2mM L-glutamine, 10U/ml Penicillin, and 10µg/ml Streptomycin and incubated at 37°C with 5% CO<sub>2</sub>.

### *Antibody Staining*

Cells were fixed on ice for 10m with 1.6% paraformaldehyde. Fixed cells were washed twice with PBS and permeabilized with ice cold 90% methanol. Fixed and permeabilized cells were washed 3x with PBS and blocked for 1h at room temperature with blocking buffer (3% BSA, 0.3% Triton-X-100 in PBS). The following primary antibodies were used: anti-Cleaved Caspase 8 (Cell Signaling

Technologies, clone D5B2), anti-Cleaved Caspase 3 (Cell Signaling Technologies, clone D175), phospho-STING (Cell Signaling Technologies, clone D1C4T), anti-TNF $\alpha$  (Biolegend, clone MP6-XT22), anti-Ki-67 (Biolegend, clone 16A8). Cells were stained with primary antibodies diluted in blocking buffer overnight at 4 $^{\circ}$  C. Primary stained cells were washed 3x with blocking buffer then incubated with secondary antibodies for 1h at room temperature, light protected. Secondary stained cells were washed 3x with blocking buffer, twice with PBS, and counterstained with DAPI. For DISC proximity ligation experiments, cells were cultured on collagen and fibronectin coated glass slides, then fixed, permeabilized, and stained as above with the following antibodies: mouse anti-Caspase 8 (Proteintech, 2B9H8) and rabbit anti-Traf2 (Abcam, EPR6048). To perform proximity ligation, we used the DuoLink In Situ Proximity Ligation Assay Kit (Sigma Aldrich).

## **Acknowledgments**

Jennifer and Alon Oyler-Yaniv significantly contributed to this chapter of my thesis by guiding me through both experiments and analysis.

## **References**

- Duggal, N. K. & Emerman, M. Evolutionary conflicts between viruses and restriction factors shape immunity. *Nat. Rev. Immunol.* 12, 687–695 (2012).
- Elde, N. C. & Malik, H. S. The evolutionary conundrum of pathogen mimicry. *Nat. Rev. Microbiol.* 7, 787–797 (2009).
- Murray, P. J. & Wynn, T. A. Protective and pathogenic functions of macrophage subsets. *Nat. Rev. Immunol.* 11, 723–737 (2011).
- Fensterl, V., Chattopadhyay, S. & Sen, G. C. No love lost between viruses and interferons. *Annu. Rev. Virol.* 2, 549–572 (2015).
- Barber, G. N. Host defense, viruses and apoptosis. *Cell Death Differ.* 8, 113–126 (2001).
- Kash, J. C. et al. Genomic analysis of increased host immune and cell death responses induced by 1918

influenza virus. *Nature* 443, 578–581 (2006).

Baskin, C. R. et al. Early and sustained innate immune response defines pathology and death in nonhuman primates infected by highly pathogenic influenza virus. *Proc. Natl Acad. Sci. USA* 106, 3455–3460 (2009).

Cillóniz, C. et al. Lethal influenza virus infection in macaques is associated with early dysregulation of inflammatory related genes. *PLoS Pathog.* 5, e1000604 (2009).

Subramanian, G. et al. A new mechanism of interferon's antiviral action: induction of autophagy, essential for paramyxovirus replication, is inhibited by the interferon stimulated gene, TDRD7. *PLoS Pathog.* 14, e1006877 (2018).

Benedict, C. A. Viruses and the TNF-related cytokines, an evolving battle. *Cytokine Growth Factor Rev.* 14, 349–357 (2003).

Brenner, D., Blaser, H. & Mak, T. W. Regulation of tumour necrosis factor signalling: live or let die. *Nat. Rev. Immunol.* 15, 362–374 (2015).

Croft, M., Benedict, C. A. & Ware, C. F. Clinical targeting of the TNF and TNFR superfamilies. *Nat. Rev. Drug Discov.* 12, 147–168 (2013).

Oyler-Yaniv, J., Oyler-Yaniv, A., Maltz, E., & Wollman, R. (2021). TNF controls a speed-accuracy tradeoff in the cell death decision to restrict viral spread. *Nature communications*, 12(1), 1-11.

## Conclusion

This dissertation explored the relationship between latent information stored within cells and its phenotypic consequences. In Chapter 1, I present a new data-driven method calculating the mutual information between high-dimensional, multimodal single cell data. I specifically quantify the relationship between transcript abundances for 83 genes and  $\text{Ca}^{2+}$  signal dynamics, concluding that there is significant shared information redundantly distributed in gene sets. These results represent quantitative support of the central dogma of biology which reconciles questions about the apparent lack of correlation between mRNA and protein counts. This method is a general approach that can be applied to any high dimensional data, adding a powerful new tool to quantify arbitrarily complex relationships within cells. In chapter 2, I present my experimental



work on TNF-induced apoptosis in the context of viral infection. The timelapse microscopy and immunofluorescence required application of computer vision techniques for segmentation, registration, and tracking. Analysis of the caspase 8 dynamics demonstrates a useful application of machine learning to find human-interpretable features of the data, allowing prediction of cell death hours before it is fully apparent. Overall these chapters demonstrate the value of data-driven methods to uncover relationships in complex biological data.